Application of DENSE-MR-Elastography to the Human Heart

Benjamin Robert,* Ralph Sinkus, Jean-Luc Gennisson, and Mathias Fink

Typically, MR-elastography (MRE) encodes the propagation of monochromatic acoustic waves in the MR-phase images via sinusoidal gradients characterized by a detection frequency equal to the frequency of the mechanical vibration. Therefore, the echo time of a conventional MRE sequence is typically longer than the vibration period which is critical for heart tissue exhibiting a short T_2. Thus, fast acquisition techniques like the so-called fractional encoding of harmonic motions were developed for cardiac applications. However, fractional encoding of harmonic motions is limited since it is two orders of magnitude less sensitive to motion than conventional MRE sequences for low-frequency vibrations. Here, a new sequence is derived from the so-called displacement encoding with stimulated echoes (DENSE) sequence. This sequence is more sensitive to displacement than fractional encoding of harmonic motions, and its spectral specificity is equivalent to conventional MRE sequences. The theoretical spectral properties of this new motion-encoding technique are validated in a phantom and excised pork heart specimen. An excellent agreement is found for the measured displacement fields using classic MRE and displacement encoding with stimulated echoes MRE (8% maximum difference). In addition, initial in vivo results on a healthy volunteer clearly show propagating shear waves at 50 Hz. Thus, displacement encoding with stimulated echoes MRE is a promising technique for motion encoding within short T_2* materials. Magn Reson Med 62:1155–1163, 2009. © 2009 Wiley-Liss, Inc.

Key words: Fast MR-elastography; motion encoding; low frequency mechanical vibrations; in vivo heart; short T_2* tissues

One of the mainstreams in medical and clinical research is the development of cardiac diagnostic tools. Echocardiography and MRI (1) are routinely used to analyze the valves' behavior, to evaluate the heart chambers' size, or to analyze the heart segments' synchronization. However, most of the diagnostic conclusions rely on quantitative measurements and parameters that are indirectly linked to pathology. For instance, myocardial viability can be accurately assessed using delayed contrast-enhanced MRI (2,3). However, new diagnostic methods are developed in order to access physical parameters characterizing the cardiac tissues such as the mechanical properties. Actually, the mechanical parameters of the myocardium have been shown to be modified by a myocardial infarct by using strain imaging in MRI (4).

MRI strain imaging estimates the heart deformation during the heart cycle by either using tagging sequences (5,6) or displacement encoding with stimulated echoes (DENSE) sequences (7). However, according to Hooke's law, strain imaging does not provide insight into the viscoelastic parameters without the corresponding stress measurement.

To measure the viscoelastic properties of the myocardium and more generally of soft tissues, an external shaker is used to generate a mechanical monochromatic excitation. As the propagation of a monochromatic wave is modeled by the equation of propagation within a viscoelastic material, the viscoelastic properties can be obtained via assessment of the displacement. Acquiring images of propagating waves is the principle of dynamic elastography using MRI (8) or ultrasound imaging (9,10). Dynamic MR-elastography (MRE) has been successfully applied, for instance, to breast (11,12), liver (13–15), and brain (16–18). Transient ultrasound-elastography has been successfully applied to breast (19) and liver (20).

The adaptation of MRE to the heart raises several distinct challenges. The echo time (TE) of an effective cardiac MRE sequence must not last more than 5 ms because of the short spin-spin relaxation time ($T_2 \sim 50$ ms for $B_0 = 1.5$ T) and a short T_2* (T_2* ~ 20 ms). An important type of MRE sequence is based on a spin echo sequence that is sensitized to motion by applying two bipolar motion sensitizing gradients (MSG), which are placed before and after the π pulse. To maximize the sequence sensitivity to the externally induced monochromatic wave, the bipolar gradients and the mechanical excitation have the same frequency (8). Thus, the TE of the MRE sequence is at least twice as long as the mechanical excitation period, which means that the lowest detectable frequency for cardiac applications would be 400 Hz if a spin echo MRE sequence (SE-MRE) were used. Therefore, MRE sequences based upon gradient echo sequences (GE-MRE) have been developed in order to obtain shorter TEs. Typically, GE-MRE contains only one MSG, which lasts only one mechanical period (21). Thus, the lowest detectable frequency would be at least 200 Hz.

However, the use of externally induced high frequency mechanical excitation is challenging for cardiac MRE applications. In general, the attenuation of mechanical waves increases strongly with frequency in biologic tissue. Thus, the utilization of high-frequency waves is prohibitive because they barely reach the heart, or at least they lose too much amplitude to provide sufficient signal in order to reconstruct reliable elastograms. Therefore, the so-called fractional encoding of harmonic motions (FEHM) sequence has been proposed (22,23) in order to use low-frequency waves in conjunction with a short TE. Here, for instance, a 50-Hz monochromatic wave is encoded via a 500-Hz MSG integrated into a gradient echo sequence. Although this technique has the potential to detect low-frequency waves within the septum, its spectral specificity

Laboratoire Ondes et Acoustique, ESPCI, Paris, France

*Correspondence to: Benjamin Robert, Laboratoire Ondes et Acoustique, ESPCI, 10 rue Vauquelin, 75005 Paris, France. E-mail: benjamin.robert@espci.fr

Received 5 May 2008; revision received 24 May 2009; accepted 28 May 2009.
DOI 10.1002/mrm.22124
Published online 24 September 2009 in Wiley InterScience (www.interscience.wiley.com).

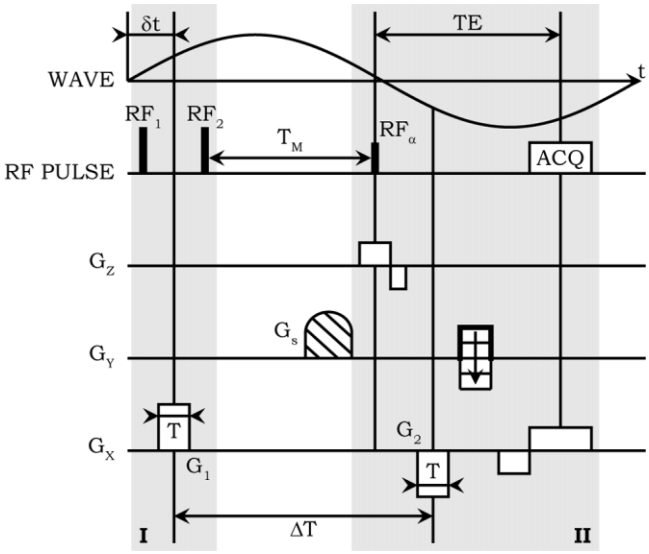

FIG. 1. DENSE-MRE sequence for an arbitrary monochromatic mechanical excitation. The motion is encoded during the preparation part I and the acquisition part II via two MSGs G_1 and G_2. A spoiler gradient G_S is applied to scramble the remaining M_{xy} within the transverse plane. The duration of ΔT is linked to the detection frequency f_0 as $\Delta T = (k + 1/2)/f_0$.

is broadband: the contribution of, for instance, a 100-Hz elastic wave to the MRI phase is stronger than for a 50-Hz elastic wave.

In this paper, we propose a novel MRE sequence that is adapted from the so-called DENSE sequence (24). DENSE has been also proven as a reliable tool for encoding static displacements within phantom and ex vivo canine kidney (25). Here, we propose to use a DENSE sequence in combination with a steady-state sinusoidal mechanical excitation such that the encoding part of the DENSE sequence is synchronized to the frequency of the external vibration. The novelty is that the motion-encoding part is thus disconnected from the MR data acquisition part, thereby enabling the encoding of relatively low-frequency waves (around 50 Hz) with a short TE. The spectral properties of this new motion-sensitive sequence are analyzed theoretically and experimentally estimated in a polyvinyl alcohol (PVA) phantom (26). The experimental spectral properties confirm the theoretical spectral properties. In addition, experiments were conducted on excised pork heart specimen to compare the motion estimation using SE-MRE and DENSE-MRE. Finally, in vivo experiments on a healthy volunteer were made to demonstrate the feasibility of DENSE-MRE in the human heart.

Theory

The proposed DENSE-MRE sequence is divided into two parts (Fig. 1): the preparation part I encodes partly the motion, while the acquisition part II is retrieving the encoded data. The preparation part I starts with a π/2 block-pulse (radiofrequency$_1$) along the (x') direction (all coordinate axes are considered to be in the rotating frame), orienting the magnetization M along the y' direction. A phase-dispersion Φ_1 is thus introduced along the desired motion-encoded direction by applying a rectangular gradient G_1 (here along the x direction). The transverse magnetization M_{xy} is now partly flipped back along the z-direction by a second π/2 block-pulse (radiofrequency$_2$) along the (-x') direction. The current longitudinal magnetization is preserved from the spin-spin relaxation T_2, and a spoiler gradient G_s is applied along the y' direction to destroy the remaining in-plane magnetization. As the magnetization time evolution is described by the Bloch equations and utilizing the fact that the duration of the preparation part I (~ 2 ms) is negligible compared to the relaxation time T_2 (~ 30 ms for $B_0 = 1.5$ T), the longitudinal magnetization M_z can be evaluated at the end of the preparation part I as:

$$M_z = M \cdot \cos\Phi_1 \quad [1]$$

where M is the longitudinal steady-state magnetization before it is flipped in the transverse plane by the block-pulse of the preparation part I. During the mixing time interval T_M between the preparation part I and the acquisition part II, the spin-lattice relaxation alters the longitudinal magnetization M_z as follows:

$$M_z = (M \cdot \cos\Phi_1 - M_0) \cdot e^{-T_M/T_1} + M_0 \quad [2]$$

where M_0 is the equilibrium magnetization and T_1 is the spin-lattice relaxation time.

The acquisition part II is now based on a gradient echo sequence with a slice-selective radiofrequency pulse (radiofrequencyα). After the longitudinal magnetization M_z has been flipped in the transverse plane with an angle α, a phase dispersion Φ_2 is introduced by applying a second gradient G_2 in the same direction as G_1. The in-plane magnetization M_{xy} can thus be evaluated and decomposed as in (23):

$$M_{xy} = \frac{M}{2} e^{-T_M/T_1} \sin\alpha \cdot e^{i\Delta\Phi} + \frac{M}{2} e^{-T_M/T_1} \sin\alpha \cdot e^{i\Sigma\Phi} + M_0(1 - e^{-T_M/T_1}) \sin\alpha \cdot e^{i\Phi_2} \quad [3]$$

where the three terms correspond to three echoes in k-space: a $\Delta\Phi = \Phi_2 - \Phi_1$ echo, a $\Sigma\Phi = \Phi_2 + \Phi_1$ echo and a Φ_2 echo. Conventional imaging gradients are applied after G_2 for data acquisition. Thus, the TE of this sequence is only limited by the duration of G_2 and the timing of the classic gradient echo imaging objects and is not linked anymore to the mechanical excitation frequency. This has been achieved by encoding part of the motion during the preparation part I and by storing the magnetization along the longitudinal direction where it relaxes as a function of T_1.

To furthermore analyze the nature of the three echoes and their location within the k-space, an estimation of the phase dispersions Φ_1 and Φ_2 is needed. The spins are considered in a mechanical steady state which corresponds to spins oscillating with amplitude x_1 around their equilibrium position x_0 and a phase $2\pi \cdot f_v t + \phi$ where f_v is the mechanical excitation frequency and ϕ a constant phase offset. The phase dispersion Φ induced by a rectangular gradient can be evaluated as:

$$\Phi = \int_0^T \gamma \cdot G(t) \cdot [x_0 + x_1 \sin(2\pi f_v t + \varphi)] \cdot dt \qquad [4]$$

where γ is the protons gyromagnetic ratio, G is the gradient strength and T is the gradient duration. The MSG G_1 is applied for $t \in [0; T]$ and G_2 for $t \in [\Delta T; \Delta T + T]$. Both gradients have the same strength with opposite signs ($G_2 = -G_1$) and the same duration T. Thus, the phase dispersions Φ_1 and Φ_2 can be evaluated accordingly:

$$\Phi_1 = \gamma G_1 x_0 T + \frac{\gamma G_1 x_1}{\pi f_v} \cdot \sin(\pi f_v T + \varphi) \cdot \sin(\pi f_v T), \quad [5]$$

$$\Phi_2 = \gamma G_2 x_0 T + \frac{\gamma G_2 x_1}{\pi f_v} \cdot \sin(\pi f_v T + 2\pi f_v \Delta T + \varphi) \cdot \sin(\pi f_v T). \quad [6]$$

In DENSE-MRE, it is favorable to choose $\Delta T = (k + 1/2) \cdot T_0$ with k an unsigned integer and T_0 the period of the detected mechanical excitation ($T_0 = 1/f_0$). Thereby, the total phase dispersions $\Sigma\Phi$ and $\Delta\Phi$ become

$$\Sigma\Phi = 2\frac{\gamma G_1 x_1}{\pi f_v} \cdot \sin(\pi f_v T) \cdot \sin\left(\frac{\pi}{2}\frac{f_v}{f_0}\right) \cdot \sin\left(\pi f_v T + \frac{\pi}{2}\frac{f_v}{f_0} + \varphi - \frac{\pi}{2}\right), \quad [7]$$

$$\Delta\Phi = 2\gamma G_1 x_0 + 2\frac{\gamma G_1 x_1}{\pi f_v} \cdot \sin(\pi f_v T) \cdot \sin\left(\frac{\pi}{2}\frac{f_v}{f_0}\right) \cdot \sin\left(\pi f_v T + \frac{\pi}{2}\frac{f_v}{f_0} + \varphi\right) \quad [8]$$

if $k = 0$. If the mechanical frequency f_v is equal to the detection frequency f_0, Eqs. [7, 8] turn into:

$$\Sigma\Phi = 2\frac{\gamma G_1 x_1}{\pi f_v} \cdot \sin(\pi f_v T) \cdot \sin(\pi f_v T + \varphi), \qquad [9]$$

$$\Delta\Phi = 2\gamma G_1 x_0. \qquad [10]$$

Thus, the $\Sigma\Phi$ echo corresponds linearly to the motion induced by the external transducer, while the $\Delta\Phi$ echo corresponds only to the spins location. Moreover, if the readout gradient is encountered, it should be noted that the $\Sigma\Phi$ echo is centered in the acquired k-space. The Φ_2 echo is translated in the acquired k-space to a position proportional to the strength of the MSG G_2 and the size of the field of view. The $\Delta\Phi$ echo is translated to a position linked to the strength of the MSG G_2 and twice the size of the field of view. Furthermore, by applying strong enough gradient (24), the $\Delta\Phi$ echo, as well as the Φ_2 echo, is shifted out of the acquired k-space. Thus, the reconstructed images contain only information that originates from the $\Sigma\Phi$ echo.

DENSE-MRE is characterized by a spectral sensitivity and a spectral specificity because its phase value depends on the detection frequency f_0 and the mechanical frequency f_v. The spectral sensitivity is defined as the maximum of the acquired phase value when the frequency f_v is equal to the frequency f_0. The spectral specificity is defined as the maximum of the acquired phase value when the frequency f_v differs from the frequency f_0. Thus, the DENSE-MRE spectral sensitivity Φ_{DM} is found by maximizing Eq. [9] with respect to the arbitrary phase offset ϕ. The solution is easily found by setting the only term containing the phase offset ϕ in Eq. [9] to identity, i.e.,

$$\Phi_{DM} = \left| 2\frac{\gamma G_1 x_1}{\pi f_v} \cdot \sin(\pi f_v T) \right| \quad \text{if } f_v = f_0. \qquad [11]$$

The DENSE- MRE spectral specificity $\delta\Phi_{DM}$ is deduced by maximizing Eq. [7] again with respect to the arbitrary phase offset ϕ. Similarly, we find:

$$\delta\Phi_{DM} = \left| 2\frac{\gamma G_1 x_1}{\pi f_v} \cdot \sin(\pi f_v T) \cdot \sin\left(\frac{\pi f_v}{2 f_0}\right) \right| \quad \text{if } f_v \neq f_0. \quad [12]$$

The performance of this novel sequence is compared to those sequences already established within the elastographic community, i.e., the GE-MRE and the SE-MRE sequences. In addition, the spectral properties of FEHM (22) are also compared to DENSE-MRE where FEHM encodes low-frequency motion within a short T_2* tissue.

The GE-MRE spectral sensitivity Φ_{GM} and its spectral specificity $\delta\Phi_{GM}$ were introduced in Muthupillai et al. (21) and Sack et al. (27):

$$\Phi_{GM} = \left| \frac{\gamma G_0 x_1}{2 f_v} \right| \quad \text{if } f_v = f_0, \qquad [13]$$

$$\delta\Phi_{GM} = \left| \frac{\gamma G_0 x_1}{\pi} \frac{f_0}{f_v^2 - f_0^2} \cdot \sin\left(\pi \frac{f_v}{f_0}\right) \right| \quad \text{if } f_v \neq f_0. \quad [14]$$

The SE-MRE spectral properties can be estimated similarly to the GE-MRE spectral properties. However, it should be noted that the SE-MRE phase dispersion is equal to the sum of two phase dispersions induced by two MSGs spaced by a time interval $\Delta t = k.T_0/2$ with k a nonzero unsigned integer. The SE-MRE spectral sensitivity Φ_{SM} can be evaluated out of the generalized equation given, for instance, in Muthupillai et al. (21):

$$\Phi_{SM} = \left| 2\frac{\gamma G_0 x_1}{2 f_v} \right| \quad \text{if } f_v = f_0, \qquad [15]$$

The estimation of the SE-MRE spectral specificity needs to take into account the time interval Δt. This time interval Δt leads to a SE-MRE spectral specificity $\delta\Phi_{SM}$ comparable to the generalized formula of $\delta\Phi_{GM}$ given in Sack et al. (27). However, the expression of $\delta\Phi_{SM}$ contains a new term that is due to Δt (if $k = 1$):

$$\delta\Phi_{SM} = \left| 2\frac{\gamma G_0 x_1}{\pi} \frac{f_0}{f_v^2 - f_0^2} \cdot \sin\left(\pi \frac{f_v}{f_0}\right) \cdot \sin\left(\frac{\pi f_v}{2 f_0}\right) \right| \quad \text{if } f_v \neq f_0. \quad [16]$$

Table 1
MR Imaging Parameters for SE-MRE and DENSE-MRE scans*

Experiments, sequence	PVA		Excised pork heart		In vivo human heart, DENSE-MRE
	SE-MRE	DENSE-MRE	SE-MRE	DENSE-MRE	
FOV (mm^2)	192 × 192	192 × 192	450 × 450	450 × 450	128 × 128
Matrix (pixels)	64 × 64	64 × 64	150 × 150	150 × 150	64 × 64
Voxel size (mm^3)	3 × 3 × 3	3 × 3 × 3	3 × 3 × 3	3 × 3 × 3	2 × 2 × 8
Flip angle (°)	90	20	90	20	90
Number of slices	7	1	5	1	1
Dynamic scans	8	10	8	10	4
Echo time (ms)	NA	4.4	NA	4.4	4.4
MSG strength ($mT \cdot m^{-1}$)	NA	42	NA	42	21
MSG duration (ms)	NA	2	NA	2	2

*The last three parameters are only applicable to DENSE-MRE scans.

The spectral properties of FEHM are derived from the GE-MRE properties as FEHM is based upon a GE-MRE sequence with a detuned MSG, i.e., the detection frequency f_0 is not equal to the mechanical frequency f_v. Thus, the spectral sensitivity of FEHM is described by Eq. [14] as exposed in Rump et al. (22). The spectral specificity of FEHM is also modeled by Eq. [14] as the sequence only contains one MSG.

MATERIALS AND METHODS

PVA Phantom Experiments

Experiments were conducted on a 1.5-T MRI scanner (Philips 1.5 T Achieva scanner, Eindhoven, Netherlands) using a PVA phantom, as well as excised pork hearts. The test objects were placed in a MRE dedicated system (Philips Research, Hamburg, Germany), which is able to induce mechanical vibrations via electrodynamic transducers (12).

DENSE-MRE and SE-MRE acquisitions are obtained at mechanical (f_v) and detection frequencies (f_0) with $(f_v, f_0) \in \{40, 50, 64, 80, 100, 125\}$ Hz. The induced mechanical motion amplitude from the transducer changed between frequencies due to its frequency response function. It was, however, kept identical at each frequency when comparing the different MRE sequences.

DENSE-MRE encodes motion by the spin phase. Thus, the estimation of the displacement from one acquisition gives access to the value of the displacement along one spatial direction at an arbitrary time point δt (Fig. 1) during the oscillatory cycle. It is possible to obtain a movie of the elastic waves by changing the delay between data acquisition and the beginning of mechanical vibration. Thereby, the phase value is oscillating over one period of the mechanical cycle. Such a group of acquisitions with varying trigger delay will be denoted as dynamic scans. Indeed, the phase value of the magnetization is linearly linked to the displacement value as shown in Eq. [9]. Thus, the complex-valued displacement can be estimated from the dynamic scans by computing the time Fourier transform of each voxel, considering that the experimental trapezoidal gradient can be substituted by an effective rectangular gradient. The estimation of the displacement along one direction relies on the same principle for SE-MRE or GE-MRE acquisitions.

The SE-MRE sequence parameters for the phantom experiments are summarized in Table 1. The repetition time and the TE depend on the detected frequency, as explained in Muthupillai and Ehman (8). The MSGs are applied separately in the two in-plane directions. Eight dynamic scans are acquired to estimate the phase value of each voxel. The DENSE-MRE parameters are shown in Table 1. The acquired slice using DENSE-MRE is identical to the central slice of the seven SE-MRE slices. The MSGs are applied separately in the two in-plane directions.

Spectral Properties Estimation (Experiments and Estimation)

The evaluation of the experimental spectral sensitivity is done in the PVA phantom as follows: each series of dynamic scans provide the amplitude A of the oscillating MR phase-value for each voxel. The ratio $r_{DM}(f_v, f_0 = f_v)$ of each image describes now the relative experimental sensitivity between SE-MRE and DENSE-MRE where:

$$r_{DM}(f_v, f_0 = f_v) = \left\langle \frac{A_{DM}(f_v, f_0 = f_v)}{A_{SM}(f_v, f_0 = f_v)} \right\rangle. \quad [17]$$

The theoretical spectral sensitivity of SE-MRE will be used as the reference for our measurements. Thus, we will verify whether $\Phi_{DM} = r_{DM} \cdot \Phi_{SM}$ holds (Eqs. [11, 15] respectively).

The evaluation of the experimental spectral specificity for $f_0 = 50$ Hz is done similarly. The ratio r_{SM} (f_v, $f_0 = 50$ Hz) of each image describes the relative experimental specificity of SE-MRE where:

$$r_{SM}(f_v, f_0 = 50\text{Hz}) = \left\langle \frac{A_{SM}(f_v, f_0 = 50\text{Hz})}{A_{SM}(f_v, f_0 = f_v)} \right\rangle. \quad [18]$$

The ratio r_{DM} (f_v, $f_0 = 50$ Hz) describes the relative experimental specificity of DENSE-MRE where:

$$r_{DM}(f_v, f_0 = 50\text{Hz}) = \left\langle \frac{A_{DM}(f_v, f_0 = 50\text{Hz})}{A_{SM}(f_v, f_0 = f_v)} \right\rangle. \quad [19]$$

As previously, the theoretical spectral sensitivity of SE-MRE will be used as the reference of our measurements.

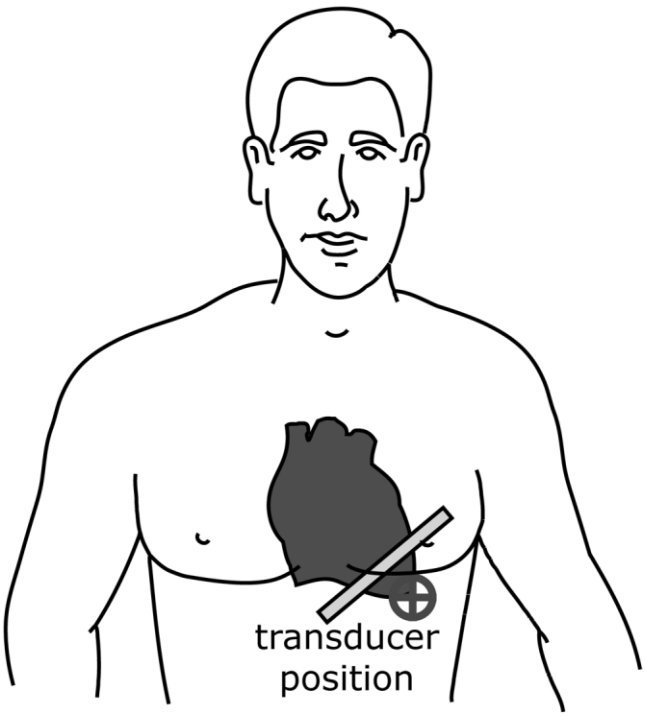

FIG. 2. Sketch of the in vivo experimental setup. The electrodynamic transducer is placed at the location of the heart apex. The acquired slice corresponds to a short-axis view.

Thus, we will estimate the experimental specificities of SE-MRE and DENSE-MRE as $\delta\Phi_{SM} = r_{SM} \cdot \Phi_{SM}$ (Eqs. [15, 16]) and $\delta\Phi_{DM} = r_{DM} \cdot \Phi_{SM}$ (Eqs. [12, 15]).

DENSE-MRE, SE-MRE and FEHM spectral properties (sensitivity, specificity) are calculated using Eqs. [11, 12], (15,16 and 14, respectively). SE-MRE is considered as the MRE "gold standard." In order to compare DENSE-MRE with FEHM for cardiac applications, FEHM TE should be equal to the DENSE-MRE TE, i.e., TE = 5 ms. Thus, the FEHM sequence is based upon a GE-MRE sequence with a 500-Hz sinusoidal MSG. The numeric parameters are: $\gamma = 2.87 \cdot 10^8$ rad $\cdot$ s^{-1} $\cdot$ T^{-1}, MSG strength $G_0 = 42$ mT $\cdot$ m^{-1}, motion amplitude $x_1 = 10$ μm, mechanical frequency $f_v \in$ [10 Hz; 800 Hz] and DENSE-MRE MSG duration $T = 2$ ms.

Feasibility Experiments for Cardiac Applications

The according SE-MRE parameters for the experiments on excised pork hearts are summarized in Table 1. The MSGs are applied in the two in-plane directions. The DENSE-MRE parameters are shown in Table 1. The acquired slice is identical to the central slice of the five SE-MRE slices. The MSGs are applied in the two in-plane directions.

Human experiments were conducted on a healthy volunteer in supine position with an electrodynamic transducer pressed against the chest as sketched in Fig. 2. A Philips SENSE cardiac coil is used with no parallel imaging and acquisition is peripheral pulse unit-triggered. A relatively low mechanical frequency $f_v = 50$ Hz was chosen in order to allow for efficient wave propagation up to the heart. The scan parameters are summarized in Table 1. The slice corresponds to a midventricular short axis view and two perpendicular saturation bands were used to avoid fold-over artifacts. An EPI readout with echo train length of 3 is used in order to acquire one dynamic scan for one motion-direction within a breath hold. Thus, one full DENSE-MRE acquisition is made in eight breath holds (25 s each) in order to acquire four dynamic scans for the two in-plane motion directions. Three sets of data are acquired in order to validate DENSE-MRE: first, MR-motion encoding without mechanical excitation; second, mechanical excitation without MR-motion encoding; and third, both MR-motion encoding and mechanical excitation are applied.

RESULTS

In DENSE-MRE, three echoes appear in the *k*-space, as shown in Eq. [3], due to the storage of the magnetization along the longitudinal direction during the mixing time T_M. The $\Sigma\Phi$ echo is proportional to the displacement amplitude, the $\Delta\Phi$ echo is proportional to the voxel position, and the Φ_2 echo is due to the T_1 relaxation. Assuming $T_1 \sim 1000$ ms in muscle for $B_0 = 1.5$ T (28), $T_M \sim 20$ ms and $M \sim M_0$, it is possible to estimate the relative contribution of the individual echoes: the Φ_2 echo corresponds to about 0.9% of the acquired in-plane magnetization M_{xy}, the $\Sigma\Phi$ echo to approximately 49.5% and the $\Delta\Phi$ echo to about 49.5%. Moreover, as shown in Kim et al. (24), the $\Delta\Phi$ echo location is out of the sampled *k*-space if strong MSGs are used. We have experimentally determined that $G_1 > 5$ mT $\cdot$ m^{-1} is sufficient in our case ($G_1 > 2.9$ rad $\cdot$ mm^{-1}). Mind that all experiments in PVA phantom or excised pork heart were conducted with $G_1 = 42$ mT $\cdot$ m^{-1} ($G_1 = 24.1$ rad $\cdot$ mm^{-1}). Thus, artifacts originating from the spin-lattice relaxation and the $\Delta\Phi$ echo are not affecting the acquired images and the acquired *k*-space contains only information originating from the $\Sigma\Phi$ echo. The same holds for the in vivo experiments which were conducted with 21 mT $\cdot$ m^{-1} MSGs ($G_1 =$ 12.1 rad $\cdot$ mm^{-1}). Moreover, it should be noted that the mixing time T_M is linked to the detection period, i.e., $T_M \sim 10$ ms for $f_0 = 50$ Hz.

The theoretical spectral sensitivities of SE-MRE, DENSE-MRE and FEHM are shown in Fig. 3 together with the experimental values obtained via Eq. [17]. The SE-MRE sensitivity is decreasing with frequency from 11.3 rad to 0.14 rad, i.e., a change by two orders of magnitude over a frequency range of two orders. The DENSE-MRE sensitivity is similarly decreasing, with frequency from 0.26 rad to 0.02 rad, i.e., by only one order of magnitude within the shown frequency bandwidth. The experimental sensitivity measured for DENSE-MRE (circles in Fig. 3) agrees very well with the theoretical curve following the predicted plateau for low frequencies (0.27 rad to 0.25 rad). This plateau, typically below $f_v < 200$ Hz, is explained by the f_v^{-1} term being balanced by the $\sin(\pi f_v T)$ term in Eq. [9]; a Taylor expansion of $\sin(\pi f_v T)$ leads to a term proportional to f_v, with $\pi f_v T$ being negligible compared to 2π ($\pi f_v T < \pi/5$ for $f_v < 200$ Hz). Contrarily, FEHM is increasing with frequency from 0.01 rad to 0.12 rad for $f_v < 420$ Hz and it is then decreasing from 0.12 rad to 0.04 rad.

The theoretical spectral specificities for a detection frequency $f_0 = 50$ Hz are shown in Fig. 4 for SE-MRE, DENSE-

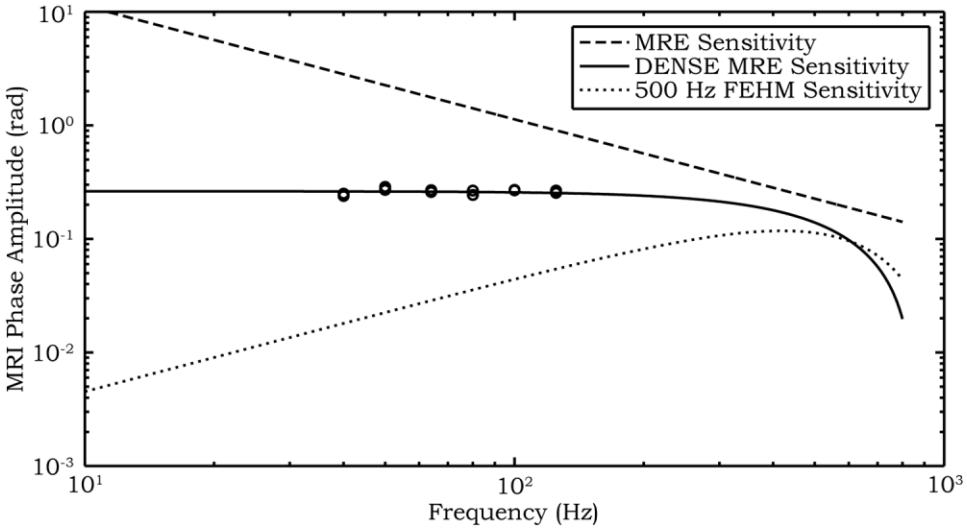

FIG. 3. Comparison of SE-MRE (dashed line), FEHM (dotted line) and DENSE-MRE (solid line) spectral sensitivities. The experimental sensitivity of DENSE-MRE is shown as circles. Numerical parameters are $\gamma = 2.87 \cdot 10^8$ rad $\cdot$ s^{-1} $\cdot$ T^{-1}, $G_0 = 42$ mT $\cdot$ m^{-1}, $x_1 = 10$ μm, $f_v \in [10$ Hz; 800 Hz], $T = 2$ ms. DENSE-MRE is less sensitive than SE-MRE, and its spectral sensitivity is constant for low frequencies. FEHM has at low frequencies an even lower sensitivity and exhibits a maximum around $f_v \sim 419$ Hz.

MRE and FEHM. The DENSE-MRE specificity is characterized by:

- a global maximum for a 50-Hz detection frequency
- local maxima for odd harmonics of the detection frequency
- zeros for even harmonics of the detection frequency

The experimental specificity of DENSE-MRE (circles in Fig. 4) clearly shows that a maximum is reached for the detection frequency $f_0 = 50$ Hz ($\delta\Phi_{DM} = \{0.25, 0.26, 0.23\}$ rad for $f_v = \{40, 50, 64\}$ Hz). The first zero of the DENSE-MRE specificity is also validated by the experiment with $\delta\Phi_{DM}$ being 20 times smaller at $f_v = 100$ Hz than at $f_v = 50$ Hz. The SE-MRE shows similarly a global maximum for $f_v \sim 45.5$ Hz and zeros for even harmonics of the detection frequency. However, odd harmonics of the detection frequency correspond also to zeros for the SE-MRE specificity. A numerical analysis of the SE-MRE spectral specificity shows indeed that the global maximum is not reached for $f_0 = f_v$, but for $f_v \sim 0.91$ f_0 ($f_v \sim 45.5$ Hz if $f_0 = 50$ Hz). The experimental values found for the SE-MRE specificity indicate a similar behavior ($\delta\Phi_{SM} = \{2.25, 2.25\}$ rad for $f_v = \{40, 50\}$ Hz). The first zero of the SE-MRE specificity is also retrieved by experiments as $\delta\Phi_{SM}$ is 100 times smaller for $f_v = 100$ Hz than for $f_v = 50$ Hz. Contrarily, the FEHM specificity does not exhibit a global maximum for a frequency equal or close to the 50-Hz detection frequency. It reaches a global maximum for $f_v \sim 419$ Hz. A numerical analysis of the GE-MRE specificity shows that the maximum value is reached for a frequency $f_v \sim 0.838$ $f_0 = 419$ Hz with here $f_0 = 500$ Hz, which was already calculated in Rump et al. (22).

Fig. 5a shows the obtained displacement amplitudes for one in-plane direction within the PVA phantom. Patterns of the displacement amplitude are closely identical when comparing SE-MRE and DENSE-MRE. More quantitatively, the relative difference ϵ between both techniques can be evaluated by:

$$\epsilon = 2 \cdot \left| \frac{\text{DENSEMRE} - \text{SEMRE}}{\text{DENSEMRE} + \text{SEMRE}} \right|. \qquad [20]$$

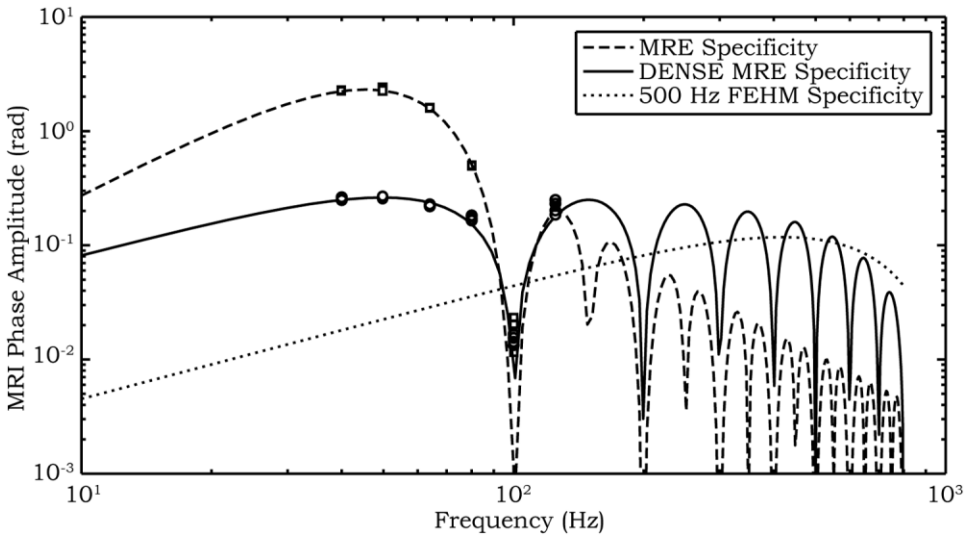

FIG. 4. Comparison of SE-MRE (dashed line), FEHM (dotted line), and DENSE-MRE (solid line) spectral specificities. The experimental specificities of SE-MRE and DENSE-MRE are shown as squares and circles respectively. Numerical parameters are $\gamma = 2.87 \cdot 10^8$ rad $\cdot$ s^{-1} $\cdot$ T^{-1}, $G_0 = 42$ mT $\cdot$ m^{-1}, $x_1 = 10$ μm, $f_v \in [10$ Hz; 800 Hz], $T = 2$ ms. DENSE-MRE spectral specificity reaches a maximum for the detection frequency f_0 like SE-MRE, and it is null for even harmonics of the detection frequency f_0. FEHM exhibits no distinct maximum at low frequencies.

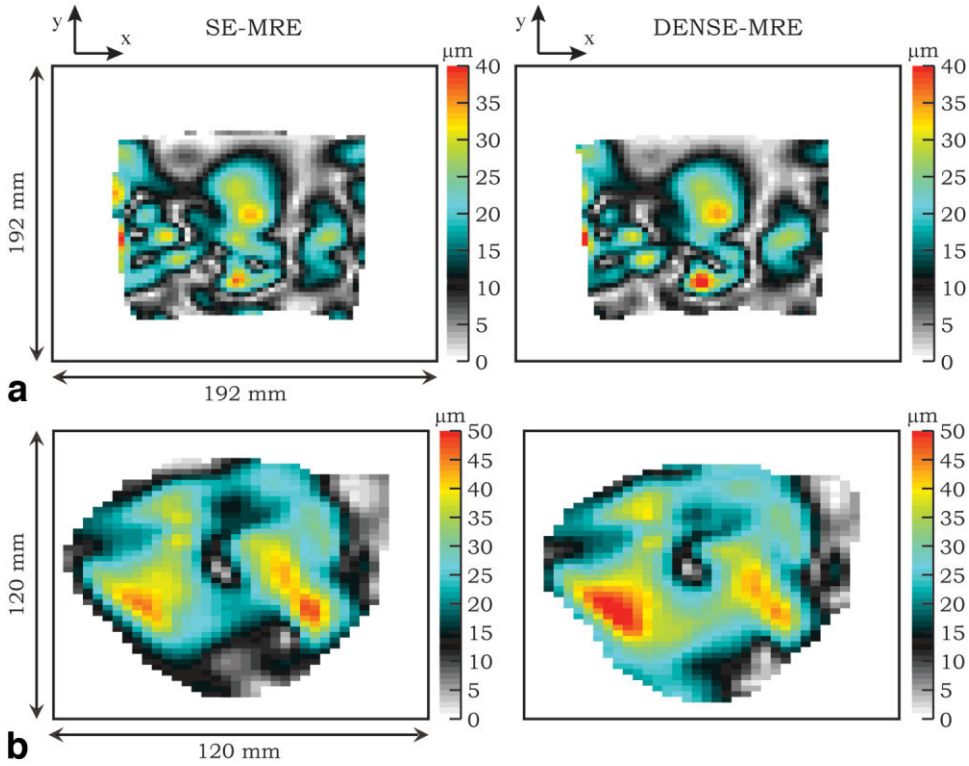

FIG. 5. **a:** Motion amplitude along the x-direction in micrometers as estimated from SE-MRE and DENSE-MRE acquisitions in a PVA phantom using mechanical excitation frequency of f_v = 100 Hz. The patterns, as well as the amplitudes, correspond very well among both acquisitions. **b:** Motion amplitude along the y-direction in micrometers is estimated out of SE-MRE and DENSE-MRE acquisitions in an excised pork heart for a mechanical frequency f_v = 100 Hz. The patterns, as well as the motion amplitudes, are almost equivalent for both acquisitions.

A relative difference ϵ of 7.7 ± 3.8% and 8.6 ± 4.3% is obtained for the displacement estimation along both directions (x-direction and y-direction) between the SE-MRE acquisition and the DENSE-MRE. This holds equally for the results obtained in the excised pork heart (Fig. 5b) and the relative differences ϵ are respectively 8.4 ± 2.7% and 8.7 ± 2.9%.

Fig. 6 shows the estimated motion amplitudes for the in-plane directions within the heart of a volunteer during the diastole (about 400 ms after the RR peak). The first set of experiments (50-Hz excitation and motion encoding) clearly shows nonzero displacement within the heart along the two in-plane directions. The motion amplitude is 23.2 ± 16,4 μm for the x-direction and 17,5 ± 14,3 μm

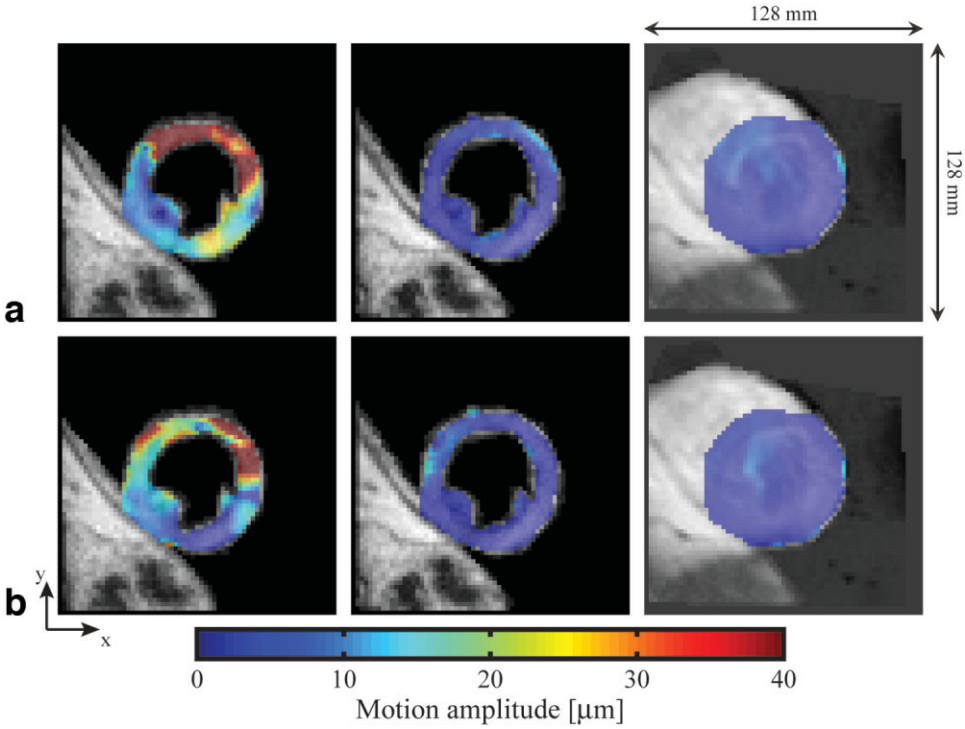

FIG. 6. Motion amplitude in micrometers is estimated out of DENSE-MRE acquisitions for a volunteer: **(a)** motion along the x-direction, **(b)** motion amplitude along the y-direction. The first map corresponds to the DENSE-MRE acquisition, the second to the no-excitation DENSE-MRE acquisition, and the third to the no-encoding DENSE-MRE acquisition.

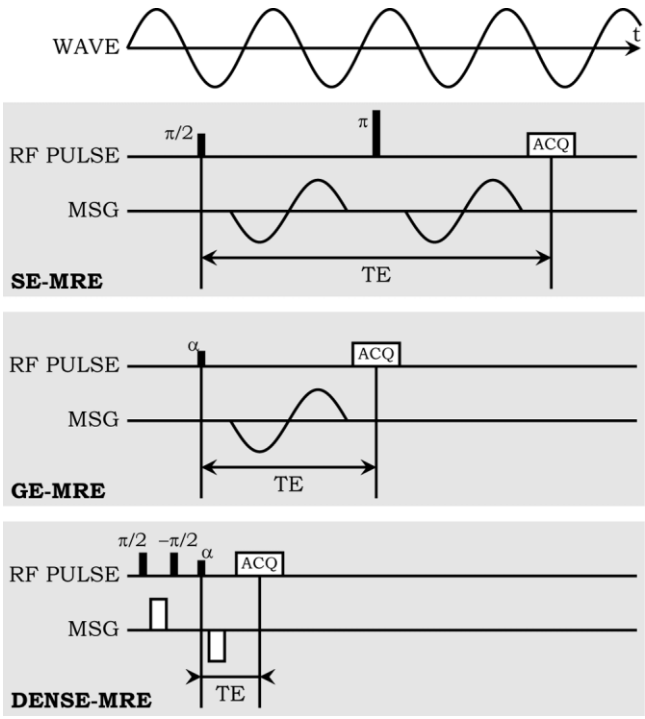

FIG. 7. Comparison of SE-MRE, GE-MRE, and DENSE-MRE in terms of TE for an arbitrary monochromatic mechanical excitation. DENSE-MRE TE is about six times smaller than the SE-MRE TE and about three times smaller than the GE-MRE TE.

for the y-direction. The second set (no excitation but motion encoding), as well as the third set (50 Hz-excitation and no motion encoding), shows statistically significant lower encoded displacements. The motion amplitudes for the second set are 3,6 ± 2,5 μm and 3.3 ± 3.0 μm, respectively, while for the third set they are 4.4 ± 2.2 μm and 3.6 ± 2.1 μm. In addition, the blood within the heart is not discriminated from the rest of the myocardium for the third set. This does not hold for the second case because motion encoding leads to signal loss in the blood pool due to its high flow pattern.

DISCUSSION

SE-MRE has proven to be a reliable technique to encode motion within soft tissues such as the breast or the liver. However, the application of SE-MRE is limited by the TE, which corresponds to approximately three times the period of the mechanical excitation as schemed in Fig. 7. The use of a 50-Hz mechanical excitation leads to a SE-MRE sequence with a TE of about 60 ms. Using GE-MRE to encode motion gives the opportunity to reach a TE about two times smaller. However, the TE for a 50-Hz excitation remains too long in order to acquire MRE data within the heart due to its short T_2*. Contrarily, the TE of DENSE-MRE is decoupled from the mechanical frequency. The TE is only limited by the duration T of the MSG G_2 (Fig. 1). For instance, TE remains 5 ms for a 50-Hz excitation as well as for a 100-Hz excitation if $T = 2$ ms. Thus, DENSE-MRE is a very promising candidate to encode low frequency motion in tissue exhibiting short T_2* values despite the 50% loss of signal due to the stimulated echoes principle as exposed in Kim et al. (24).

DENSE-MRE is however less sensitive than SE-MRE as shown in Fig. 3. Actually, SE-MRE is encoding during one TE typically two full mechanical periods, while DENSE-MRE is integrating only partially the motion during the application of the MSGs. This clearly leads to a loss in sensitivity. When comparing now DENSE-MRE to the FEHM approach, it is obvious that FEHM loses again approximately a factor of 10 in sensitivity. The FEHM sensitivity can be increased by decreasing the frequency of the MSG. However, a longer MSG duration increases the TE of the sequence, which is critical for cardiac applications. In addition, the FEHM approach does not provide a maximum for the spectral specificity at the mechanical driving frequency (Fig. 4). This aspect can be critical for cardiac applications as multifrequency elastic waves are generated naturally in the heart. For instance, Kanai (29) used the aortic-valve closure at the end of systole to estimate viscoelastic properties of the myocardium for one particular cardiac phase. On the contrary, SE-MRE and DENSE-MRE sequences are frequency discriminative, with a global maximum at a frequency close to the mechanical excitation frequency. The global maximum for SE-MRE is indeed reached for a frequency smaller than the detection frequency. Thus, DENSE-MRE has a maximal encoding for the detection frequency contrarily to FEHM, GE-MRE or even SE-MRE.

DENSE-MRE can be considered as a "classic" GE-MRE or SE-MRE sequence characterized by a noninteger number of MSGs. Denoting Φ_{GM} (Eq. [14]) with one MSG as the base unit, the corresponding generalized phase value for the motion sensitive sequences is:

$$\Phi = n \cdot \Phi_{GM} \qquad [21]$$

with n equal to the number of MSGs. Thus, for SE-MRE $n = 2$ and $n = 4/\pi \cdot \sin(\pi f_v T)$ for DENSE-MRE (see Eqs. [11, 15]). Therefore, data processing is identical between SE-MRE and DENSE-MRE. For instance, the amplitude maps shown in Fig. 5 for DENSE-MRE have been obtained with $n = 0.748$ (corresponding to $T = 2$ ms, $f_v = 100$ Hz). The resulting maps of the displacement are similar in terms of motion amplitude and motion patterns when compared to SE-MRE. Thus, viscoelastic parameters can be estimated from DENSE-MRE acquisitions using the same algorithms as for SE-MRE acquisitions.

The in vivo experiments prove the feasibility of cardiac DENSE-MRE: clearly, nonzero motion amplitudes are estimated within the myocardium wall and the viscoelastic properties of the myocardium could be evaluated as the wall thickness corresponds to about 10 voxels, i.e., the number of voxels is sufficient to use spatial derivatives in order to calculate the viscoelastic parameters. The control experiments (2nd and 3rd set in Fig. 6) demonstrate that the DENSE-MRE pulse sequence is relatively insensitive to displacement of the heart without transducer excitation and transducer excitation without motion encoding.

CONCLUSIONS

This study introduces DENSE-MRE as an effective new method to acquire elastic wave propagation. A theoretical

analysis of DENSE-MRE and a comparison with existing motion sensitive sequences (SE-MRE and FEHM) have been conducted. The theoretical results on the DENSE-MRE spectral properties have been confirmed by experiments in a PVA phantom using external excitations. DENSE-MRE experiments were performed in excised pork hearts in order to test the applicability of the sequence in a material exhibiting MR-properties and mechanical properties similar to those of the human heart. Moreover, in vivo experiments were conducted to prove the feasibility of cardiac DENSE-MRE for the imaging of low frequency shear wave propagation in the human heart. This provides the basis for future studies in order to estimate the viscoelastic properties of the heart wall.

DENSE-MRE is less sensitive to motion than SE-MRE, which is due to the encoding timing. Thus, DENSE-MRE is not developed as a more sensitive technique to encode motion within a medium, but it represents a solution to encode low frequency motion in a material exhibiting short T_2* values. The shortening of the TE is achieved by storing the encoded magnetization after the preparation part along the longitudinal direction. Thereby, DENSE-MRE profits from the long T_1 of the medium. Furthermore, DENSE-MRE is comparable to SE-MRE in terms of spectral specificity. This can be important in an active structure like the beating heart, which produces its own broadband spectrum of mechanical vibrations on top of an externally applied mechanical excitation.

Compared to an equivalent FEHM sequence, DENSE-MRE presents several advantages. Its spectral sensitivity is higher for low frequency mechanical excitations. In particular, elastographic applications to the heart necessitate utilization of low-frequency excitations because the attenuation of acoustic waves increases typically with frequency in soft tissues (12,30). Moreover, DENSE-MRE is a more frequency-discriminative sequence than FEHM because FEHM is based on the spectral specificity of a GE-MRE with a high detection frequency, while DENSE-MRE is centered on the detection frequency.

Thus, compared to existing motion encoding sequences, DENSE-MRE represents a promising technique to estimate the viscoelastic properties of in vivo human heart tissues. Furthermore, the in vivo experiments show feasibility that cardiac DENSE-MRE examinations can be conducted within eight breath-holds in less than 4 min.

REFERENCES

1. Duerinckx AJ. Cardiac MRI for clinicians: an overview. Int J Cardiovasc Imaging 2001;17:437–443.
2. Kim RJ, Wu E, Rafael A, Chen EL, Parker MA, Simonetti O, Klocke FJ, Bonow RO, Judd RM. The use of contrast-enhanced magnetic resonance imaging to identify reversible myocardial dysfunction. N Engl J Med 2000;343:1445–1453.
3. Choi K, Kim RJ, Gubernikoff G, Vargas JD, Parker M, Judd RM. Transmural extent of acute myocardial infarction predicts long-term improvement in contractile function. Circulation 2001;104:1101–1107.
4. Gupta KB, Ratcliff MB, Fallert MA, Edmunds LH, Bogen DK. Changes in passive mechanical stiffness of myocardial tissue with aneurysm formation. Circulation 1994;89:2315–2326.
5. Zerhouni EA, Parish DM, Rogers WJ, Yang A, Shapiro EP. Human heart: tagging with MR Imaging–a method for noninvasive assessment of myocardial motion. Radiology 1988;169:59–63.
6. Liu W, Chen J, Ji S, Allen JS, Bayly PV, Wickline SA, Yu X. Harmonic phase MR tagging for direct quantification of Lagrangian strain in rat hearts after myocardial infarction. Magn Reson Med 2004;52:1282–1290.
7. Aletras AH, Ding S, Balaban RS, Wen H. DENSE: Displacement encoding with stimulated echoes in cardiac functional MRI. J Magn Reson 1999;137:247–252.
8. Muthupillai R, Ehman RL. Magnetic resonance elastography. Nat Med 1996;2:601–603.
9. Parker KJ, Huang SR, Musulin RA, Lerner RM. Tissue response to mechanical vibrations for "sonoelasticity imaging". Ultrasound Med Biol 1990;16:241–246.
10. Sandrin L, Tanter M, Gennisson JL, Catheline S, Fink M. Shear elasticity probe for soft tissues with 1D transient elastography. IEEE Trans Ultrason Ferroelec Freq Control 2002;49:436–446.
11. Sinkus R, Lorenzen J, Schrader D, Lorenzen M, Dargatz M, Holz D. High-resolution tensor MR-elastography for breast tumor detection. Phys Med Biol 2000;45:1649–1664.
12. Sinkus R, Siegmann K, Xydeas T, Tanter M, Claussen C, Fink M. MR elastography of breast lesions: understanding the solid/liquid duality can improve the specificity of contrast-enhanced MR mammography. Magn Reson Med 2007;58:1135–1144.
13. Rouvière O, Yin M, Dresner MA, Rossman PJ, Burgart LJ, Fidler JL, Ehman RL. MR elastography of the liver: preliminary results. Radiology 2006;240:440–448.
14. Huwart L, Seminpoux C, Vicaut E, Salameh N, Annet L, Danse E, Peeters F, Ter Beek LC, Rahier J, Sinkus R, Horsmans Y, Van Beers BE. Magnetic resonance elastography for the noninvasive staging of fibrosis. Gastroenterology 2008;135:32–40.
15. Asbach P, Klatt D, Hamhaber U, Braun J, Somasundaram R, Hamm B, Sack I. Assessment of liver viscoelasticity using multifrequency MR elastography. Magn Reson Med 2008;60:373–379.
16. Green MA, Bilston LE, Sinkus R. In vivo brain viscoelastic properties measured by magnetic resonance elastography. NMR Biomed 2008;21:755–764.
17. Sack I, Beierbach B, Hamhaber U, Klatt D, Braun J. Non-invasive measurement of brain viscoelasticity using magnetic resonance elastography. NMR Biomed 2007;21:265–271.
18. Kruse SA, Rose GH, Glaser KJ, Manduca A, Felmlee JP, Jack CR, Ehman RL. Magnetic resonance elastography of the brain. Neuroimage 2008;39:231–237.
19. Tanter M, Bercoff J, Athanasiou A, Deffieux T, Gennisson JL, Montaldo G, Muller M, Tardivon A, Fink M. Quantitative assessment of breast lesion viscoelasticity: initial clinical results using supersonic shear imaging. Ultrasound Med Biol 2008;34:1373–1386.
20. Sandrin L, Fourquet B, Hasquenoph JM, Yon S, Fournier C, Mal F, Christidis C, Ziol M, Poulet B, Kazemi F, Beaugrand M, Palau R. Transient elastography: a new non-invasive method for assessment of hepatic fibrosis. Ultrasound Med Biol 2003;29:1705–1713.
21. Muthupillai R, Rossman PJ, Lomas DJ, Greenleaf JF, Riederer SJ, Ehman RL. Magnetic resonance imaging of transverse acoustic strain waves. Magn Reson Med 1996;36:266–274.
22. Rump J, Klatt D, Braun J, Warmuth C, Sack I. Fractional encoding of harmonic motions in MR-elastography. Magn Reson Med 2007;57:388–395.
23. Rump J, Warmuth C, Braun J, Sack I. Phase preparation in steady-state free precession MR elastography. Magn Reson Imaging 2008;26:228–235.
24. Kim D, Gilson W, Kramer C, Epstein F. Myocardial tissue tracking with two-dimensional cine displacement-encoded MR-imaging: development and initial evaluation. Radiology 2004;230:862–871.
25. Chenevert TL, Skovoroda AR, O'Donnel M, Emelianov SY. Elasticity reconstructive imaging by means of stimulated echo MRI. Magn Reson Med 1998;39:482–490.
26. Chu KC, Rutt BK. Polyvinyl alcohol Cryogel: an ideal phantom material for MR studies of arterial flow and elasticity. MRM 1997;37:314–319.
27. Sack I, McGowan CK, Samani A, Lunginbuhl C, Oakden W, Plewes DB. Observation of nonlinear shear wave propagation using magnetic resonance elastography. Magn Reson Med, 2004;52:842–850.
28. Venkatesan R, Lin W. Accurate determination of spin-density and T1 in the presence of RF field inhomogeneities and flip-angle miscalibration. Magn Reson Med 1998;40:592–602.
29. Kanai H. Propagation of spontaneously actuated pulsive vibration in human heart wall and in vivo viscoelasticity estimation. IEEE Trans Ultrason Ferroelec Freq Control 2007 2005;52:1931–1942.
30. Kiss M, Varghese T, Hall T. Viscoelastic characterization of in vitro canine tissue. Phys Med Biol 2004;49:4207–4218.